International Journal of Signal Processing, Image Processing and Pattern Recognition
Vol.9, No.8 (2016), pp.39-58
http://dx.doi.org/10.14257/ijsip.2016.9.8.04

Fabric Defect Detection Using Adaptively Tuned Gabor Filters

Luo Jie[1], Hu Quan[2], Bi Mingde[3] and Ao Fei[4]

[1,2]*School of Automation, Wuhan University of Technology, China*
[3]*Department of Control Science and Engineering, Huazhong University of Science and Technology, China*
[4]*State Grid Hunan Electric Power Corporation Research Institute, China*
[1]*luo_jie@whut.edu.cn,*[2]*hq2469@126.com,*[3]*3357007@qq.com,*
[4]*graysky0821@163.com*

Abstract

A new fabric defect detection algorithm base on Gabor filters is proposed. The spectral characteristics of both fabric texture and defects are analyzed. Gabor wavelet which can be considered as a bank of Gabor filters are used for the decomposition of fabric image. Based on spectral characteristics of fabric texture and defects, a new tuning method of Gabor wavelet is proposed to enhance the energy of defective region and attenuate the energy of normal texture. Decomposition images from different scales and orientations are fused into a single one to emphasize the presence of different kinds of defects. For comparison, the performance of proposed method as well as other two other defect detection methods using Gabor filters is evaluated with typical fabric defect samples. The experiment results obtained indicate that the proposed method is more effective than the other two.

Keywords*: Fabric defect, Defect detection, Gabor wavelet, Image filtering*

1. Introduction

Fabric defect is the most important factor affecting the quality of the fabrics. It is reported that the price of the fabric decreases 45%-65% due to the presence of defects [1]. The traditional defect detection task is accomplished by human inspector, which makes the quality of fabric devoid of consistency and reliability. It is found that even a highly trained inspector can only detect about 70% of defects at a speed of 15-20 m/min [2], the inspector has to detect a fabric repeatedly to achieve 100% detection rate. As the development of computer science and image processing technology, automatic visual inspection plays an important role in industrial fabric quality assurance and many methods base on texture analysis were proposed for fabric defect detection.

The characteristic of fabric surface depends on the spatial distribution of the gray value of its pixels. Thus several spatial statistical methods were proposed as the earliest attempts (up to 90's) for fabric defect detection using fractal dimension [3-[4], morphological feature [5-6] (Mallick-Goswami and Datta, 2000; Chandra *et. al.*, 2010), and co-occurrence matrix [6]. As the statistical features characterize only the global texture pattern, they are not sensitive to the local textural variation caused by tiny defects, so that they are more efficient to detect global defects than local tiny ones. Cohen *et. al.*, [8] used the Gauss Markov random field (GMRF) to model the texture pattern of non-defective fabric image, and the defect was detected by the rejection of the model using hypothesis testing theory. More recently, as the development of the multi-resolution theory, the spectral method for visual inspection of fabric defect becomes more and more popular and is used as an alternative way to replace the statistical and model based methods. Chan and Pang [9] used Fourier transform to detect fabric defects. However because of poor its local resolution in spatial domain, it turned out to be only suitable to

ISSN: 2005-4254 IJSIP

detect global defects rather than local ones. As the Gabor filter achieves the optimal joint resolution in spatial and spectral domain, it was used for detecting local defects [11-14]. Similar to Gabor transform, the wavelet transform also provides local resolution in both spatial and spectral domains. Besides, because the wavelet basis is orthogonal or bi-orthogonal, there is no redundancy between different decomposition scales and orientations. Thus several fabric defect detection algorithms using wavelet transform were also proposed [15-17].

As suggested by psychophysical studies [18], the visual images are processed by human brain through multi-scale analysis with different frequencies and orientations. As the textural fabric images are consist of repetition of some basic texture primitives with a displacement, they exhibit high degree of periodicity along certain orientation. Thus it is suitable to use multi-scale analysis such as Gabor and wavelet transform for fabric texture characterization and defect detection.

For defect detection with multi-scale analysis, the selection of the mother wavelet (or wavelet basis), decomposition scales and orientations are the most important factors affecting the detection results. An adaptive Gabor filter [11] (wavelet basis [16]) was used to characterize each kind of defects, whose characteristics were already known as a prior knowledge, and a set of Gabor filters (wavelet basis) were used for detecting multiple kinds of the defects. This method is not proper for online inspection, where the characteristic of detects are usually unknown. Jasper *et. al.*, [15] and Yang *et. al.*, [17] designed an adaptive wavelet basis to characterize fabric texture and only one scale was used so that multi-resolution representation of the defect was not provided. Sari-Sarraf and Goddard [2] used Daubechies D2 wavelet basis and selected decomposition scale manually by human observation without automatic selection scheme.

Generally, the wavelet transform generates decomposition scales mutually orthogonal to each other, however it is not shift-invariant which means that defects appear at different location may produce different detection results. A solution to this problem is to use undedicated wavelet transform [19], which is shift-invariant but not orthogonal, to replace standard wavelet transform. However, for the wavelet basis such as Haar, Daubechies and Meyer, their pass-bands of each scale and orientation are localized at fixed points in the frequency domain, thus it is not applicable to set the center of their pass-band flexibly to specified frequency points of interest. Similar to wavelet transform, the Gabor wavelet can also produce a multi-resolution representation of images. Besides Gabor wavelet can provide a flexible scheme to set its pass-band center at arbitrary position in the frequency domain. Thus in this paper, a bank of Gabor filters called Gabor wavelets are used for multi-scale analysis. The center frequencies of the Gabor filters are tuned adaptively to the fabric texture to enhance the energy distinction between the defective and non-defective regions. And the detection results with and without the adaptive tuning scheme are provided to illustrate the improvement of the proposed method.

2. Gabor Wavelets

A two dimensional Gabor function $g(x,y)$ and its Fourier transform $G(u,v)$ can be defined as

$$g(x,y)=\frac{1}{2\pi\sigma_x\sigma_y}\exp\left[-\frac{1}{2}\left(\frac{x^2}{\sigma_x^2}+\frac{y^2}{\sigma_y^2}\right)\right]\exp(2\pi jWx) \tag{1}$$

$$G(u,v)=\exp\left\{-\frac{1}{2}\left[\frac{(u-W)^2}{\sigma_u}+\frac{v^2}{\sigma_v}\right]\right\} \tag{2}$$

Where

$$\sigma_u = \frac{1}{2\pi\sigma_x}, \sigma_v = \frac{1}{2\pi\sigma_y} \tag{3}$$

and w denotes the center frequency of the Gabor function. The space constants σ_x and σ_y define the Gaussian envelope along the x and y axes. A bank of self-similar functions referred to as Gabor wavelets can be produced by using $g(x, y)$ as the mother Gabor wavelet. By appropriate dilations and rotations of $g(x, y)$, a bank of self-similar functions can be obtained and written as

$$g_{mn}(x, y) = a^{-m} g(x', y'), \quad a > 1, \quad m, n = \text{integer} \tag{4}$$

$$x' = a^{-m}(x\cos\theta + y\sin\theta), \quad y' = a^{-m}(-x\sin\theta + y\cos\theta) \tag{5}$$

where $\theta = n\pi / N$, $n = 0, 1, \ldots N-1$, and N is the total number of orientations. $m = 0, 1, \ldots, M-1$, and M is the number of scales in the multi-scale decomposition. The scale factor a-m ensures that the energy in Equation (4) is independent of m and θ, which means all the Gabor filters defined by self-similar functions with different scales and orientation have the same energy. And the Fourier transform of $g_{m,n}(x, y)$ can be written as

$$G_{m,n}(u, v) = a^m \exp\left\{-\frac{1}{2}\left[\frac{(u'-W)^2}{\sigma_u} + \frac{v'^2}{\sigma_v}\right]\right\} \tag{6}$$

$$u' = a^m(u\cos\theta + v\sin\theta), \quad v' = a^m(-u\sin\theta + v\cos\theta) \tag{7}$$

Gabor wavelet can provide a complete but redundant representation of image and is of the property of shift-invariant [20]. Because of the non-orthogonality of the Gabor wavelet, there are redundancies between different scales and orientations. As illustrated in [21], asymmetric Gabor filters are used to reduce this redundancy for texture characterization. Let U_l, and U_h, denote the lower and upper center frequencies of interest. In order to make sure that the half-peak magnitude support of the filter responses in the frequency spectrum touch each other as illustrated in Figure 1, Equation (8-10) are used to calculate the parameters a, σ_u and σ_v in Equation (6).

$$a = (U_l / U_h)^{\frac{1}{M-1}} \tag{8}$$

$$\sigma_u = \frac{(a-1)U_h}{(a+1)\sqrt{2\ln 2}} \tag{9}$$

$$\sigma_v = \tan\left(\frac{\pi}{2N}\right)\left[U_h - 2\ln\left(\frac{2\sigma_u^2}{U_h}\right)\right]\left[2\ln 2 - \frac{(2\ln 2)^2\sigma_u^2}{U_h^2}\right]^{-\frac{1}{2}} \tag{10}$$

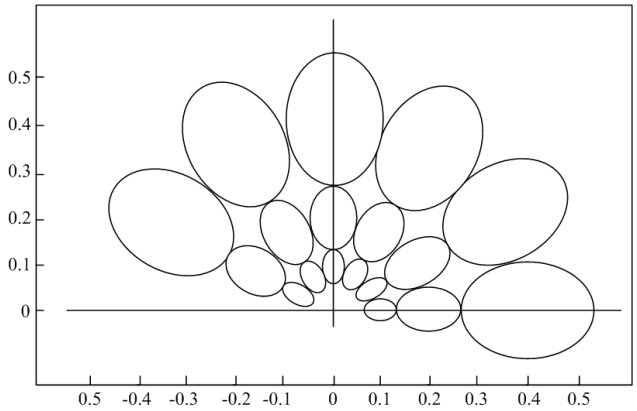

Figure 1. Frequency Response of Gabor Filter Bank with
$U_l = 0.1, U_h = 0.4, N = 6, M = 3$

Figure 1, illustrates the frequency response of a bank of Gabor filters with $U_l = 0.1, U_h = 0.4, N = 6, M = 3$. The ellipses in Figure 1 indicate the half peak magnitude of the filter responses. It can be seen that the $M \times N$ Gabor filters cover the frequency region from U_l to U_h. Along each orientation, the center frequency of filters from neighboring scales are placed an octave apart.

3. Spectral Characteristic of Fabric Texture and Defects

Figure 2, illustrates several non-defective fabric image samples of different texture patterns. It can be seen that because of the regularity in the fabric weaving process, the texture of fabric images exhibit a high degree of periodicity. That means the fabric texture has significant spectral characteristics which is indicated in its Fourier spectrum. Figure(a), shows a non-defective fabric sample which is made zero mean to suppress the zero-frequency component in its 2D Fourier spectrum as illustrated in Figure 2 (b).

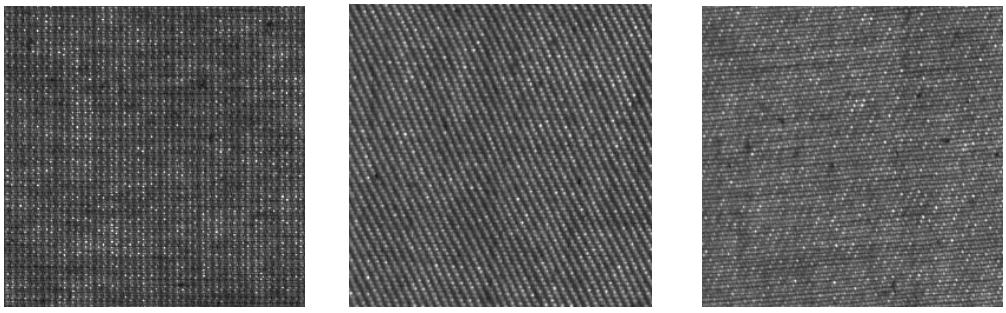

(a) (b) (c)

Figure 2. Non-Defective Fabric Defect Samples

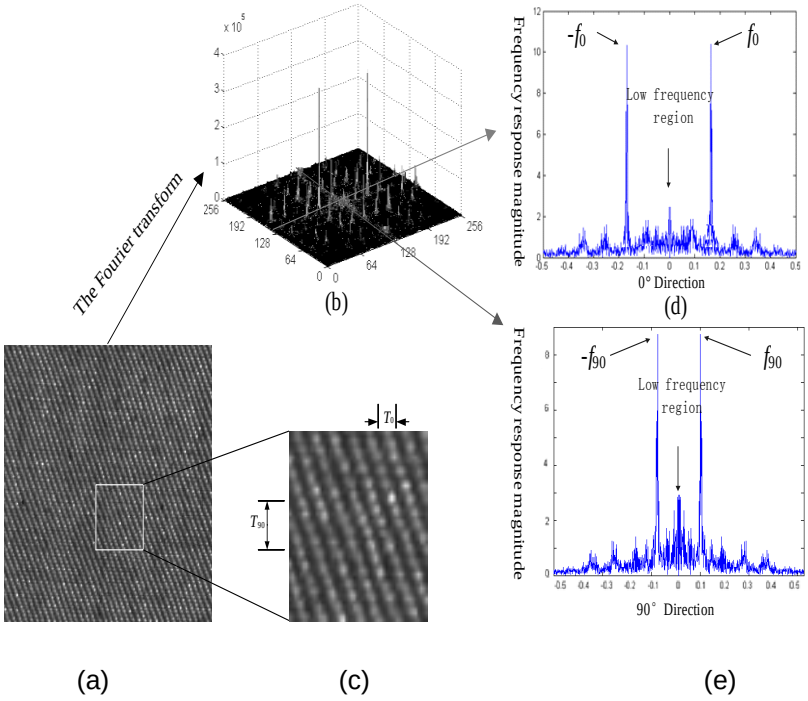

Figure 3. Spectral Characteristic of Non-Defective Fabric Texture

Because of high degree of periodicity of fabric texture, in Figure 2 (b), there are two spectral frequency response peaks, which is symmetrical to the origin of the spectral coordinate. The magnitudes of spectral frequency response in the neighboring regions centered at these two peaks are much larger than elsewhere. Thus the main energy of the fabric texture is located in the neighboring regions of these two peaks. Besides, there also exists symmetrical spectral frequency response peaks in 1D Fourier spectrum along wrap direction (0°) and fill direction (90°) as illustrated Figure 2(d), and Figure 2(e), respectively. The frequency point f_0 and f_{90}, where the response peaks are located, are the reciprocal of the texture periodicity T0 and T90 (see Figure 2(c)) along 0° and 90°. Similar to the response peaks in 2D situation, the response magnitudes nearby f_0 and f_{90} are also much larger than elsewhere in 1D Fourier spectrum. Base on descriptions above, our first argument can be acquired as

Argument A1: For fabric texture, because of its high degree of periodicity, there exists frequency response peaks in its Fourier spectrum (in both 1D and 2D format) and the main energy of the texture image is located nearby the response peaks.

Figure 4, illustrates several typical fabric defects with different texture backgrounds. It can be seen that the normal fabric texture is composed by repetition and displacement of certain texture primitive called *textel*. Because of the high degree of periodicity of fabric texture, the intensities of image pixels along each orientation keep vibrating with a certain pattern. However, the presence of defects will break this pattern. And the intensities of pixels within the defective region tend to has lower variations than the normal texture pixels.

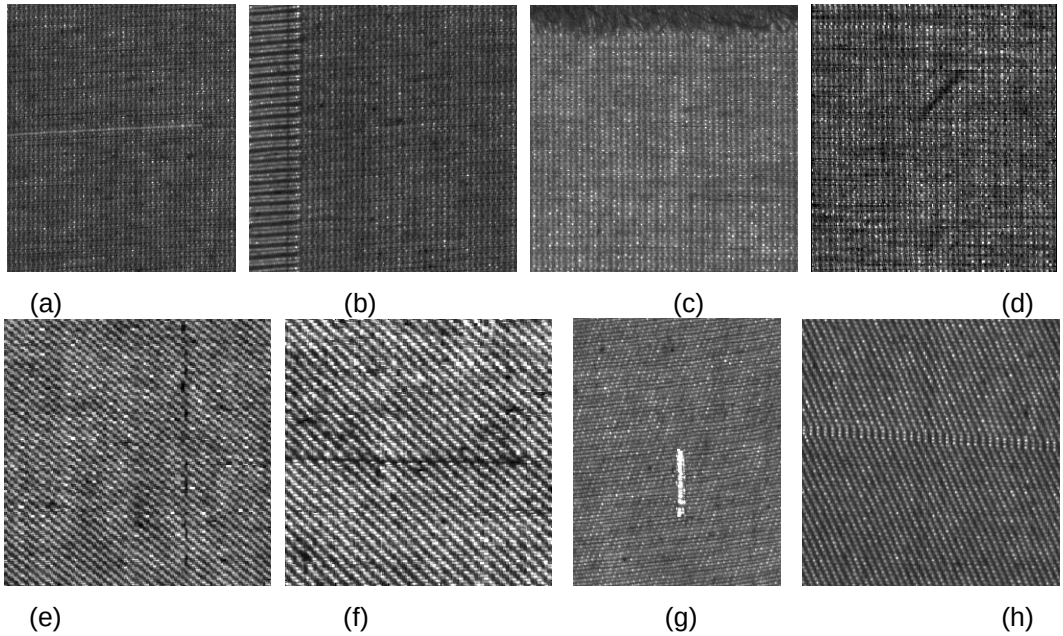

Figure 4. Defect Break-End, Miss-Yarn, Weft, Big-Knot, Slack-End, Dirty-Yarn, Miss-Pick in (a)-(h) Respectively

For fabric defects with comparative large size, such as defect weft and defect hole in Figure 4(c), (g) respectively, their texture patterns are quite different from normal texture. Especially for defect hole, with its boundary, the pixel intensities nearly keep constant (with white pixels). Thus its intensity variation is much lower than the normal texture. The intensity variation distinction between defective region and normal texture also exists in small defects such as miss-pick in Figure 4(h) and even tiny defect such as slack-end in Figure 4(e). And this distinction also indicates an important spectral characteristic of fabric defects.

Figure 5 illustrates the spectral characteristic of defect slack-end. Along 0° (wrap direction), it appears in the form of sharp transition, however along 90° (fill direction), the intensity variation of pixels in defective region are still lower than the normal texture. In Figure 5(a), two lines of both non-defective and defective pixels along 90° are marked by two white rectangles. The intensity variations of pixels within the two rectangles are illustrated in Figure 5(b), and Figure 5(c). Respectively. In Figure 5(b), the intensities of non-defective pixels keep vibrate with a certain periodicity; however in Figure 5(c), when defective pixel appears, the vibration stops and the intensity variation becomes much lower. The intensity variation distinction is also indicated in the Fourier spectrum in Figure 5(d). In intermediate and high frequency region the response of defective and non-defective pixels are nearly the same. However, in low frequency region the response of defective pixels are much larger than the non-defective ones, which means the main energy of defect is located in the lower frequency regions than the normal texture. This is because defective pixels have lower intensity variation. Figure 6 illustrates this situation for defect miss-pick. The texture pattern of the miss-pick is very similar to the normal texture, however along 90°, it also results higher low-frequency response than normal texture. Thus our second argument can be acquired as

Argument A2: For fabric defect, within its boundary, tend to have lower intensity variation than normal texture, which means the main energy of the defect lies in lower frequency region than the normal texture in the frequency domain.

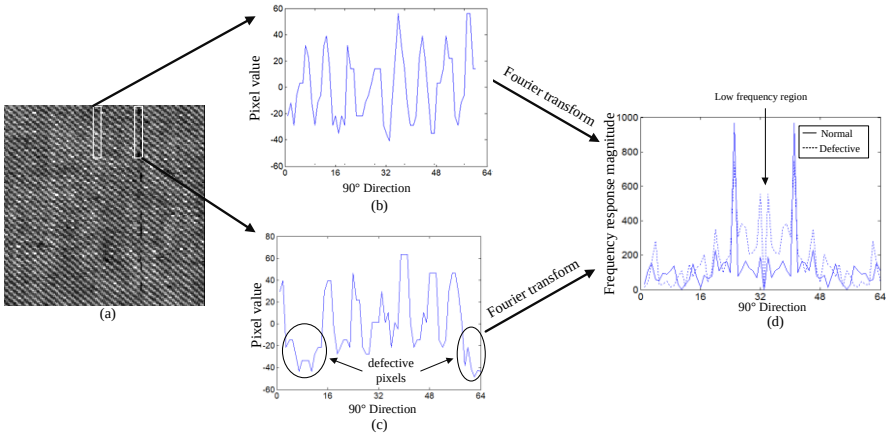

Figure 5. Spectral Characteristic of Defect Slack-End

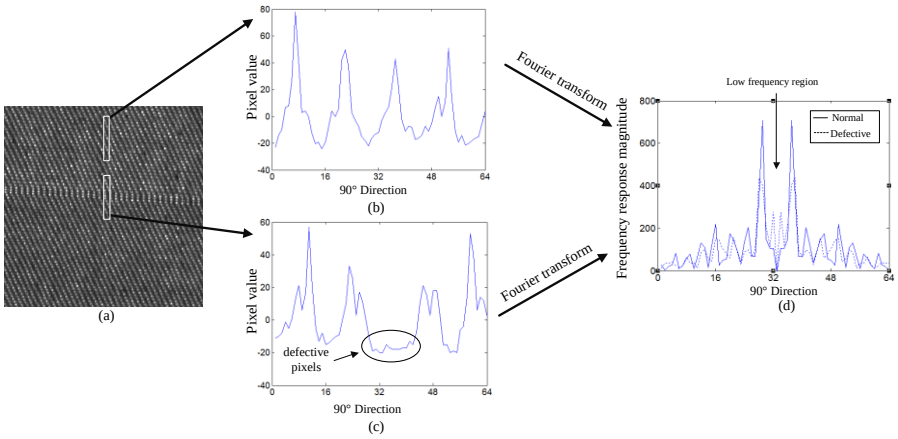

Figure 6. Spectral Characteristic of Defect Miss-Pick

4. Adaptive Tuning of Gabor Wavelet

Fabric defect detection can be considered as detection of unknown defects from the normal texture background whose characteristic has already known as a prior knowledge. The Gabor filters are tuned adaptively to the "known" fabric texture to make sure that they have low frequency responses to the normal texture but high frequency responses to the "unknown" defect. The Gabor filters are used to enhance the energy distinctions between defective regions and normal texture, which facilitates the detection of defects by thresholding. As shown in Equation (8-10) there are four parameters U_l, U_h, M, and N which should be selected for the tuning of Gabor filters. The objective tuning Gabor filters is to enhance the energy (frequency responses) of defective region and attenuate the energy (frequency responses) of normal texture in the filtered images.

4.1. Selection of U_h

As described in section2, U_h refers to as the upper boundary of the interest frequency region. According to Argument A1, the main energy of the texture image is located nearby two response peaks in its 2D Fourier spectrum. Let the localization of the response peaks be (f_u, f_v) and (-f_u, -f_v). According to Argument A2, the main energy of the defect lies in lower frequency region than the normal texture in the frequency domain. Thus the defective frequency region should be within the boundary between (f_u, f_v) and (-f_u, -f_v). In order to enhance the energy of the non-defective region, the pass-band of the Gabor filters should be also within that

boundary. Thus U_h, which denotes the upper boundary of the pass-band of Gabor filters, is set by the following formula

$$U_h = \sqrt{f_u^2 + f_v^2}$$

In order attenuate the energy of normal texture, the frequency response peaks of normal texture, which is located at (f_u, f_v) and (-f_u, -f_v), should be in the stop-band of the Gabor filters. A small modification is made to the Gabor wavelets described in SEC to meet this requirement. Let $G_{m,n}$ be the Gabor filter at scale m+1 and orientation n, where scale 0 denotes original image. All the Gabor filters in the filter bank are rotated by an angle $\varphi = \tan^{-1}(f_v / f_u)$ to make sure that the center frequency of the Gabor filter $G_{0,0}$ is located at (f_u, f_v), as illustrated in Figure 7. Then θ in Equation (5) is converted to $\theta = n\pi/K + \varphi$. The modified Gabor filters still cover the frequency region with U_h as its upper boundary but with an initiation angle φ instead of zero. The Gabor filter $G_{0,0}$ is indicated by gray color in Figure 7, with (f_u, f_v) is at its center frequency. This Gabor filter will be not involved in image filtering and will be excluded from the Gabor filter bank, because (f_u, f_v) is in its pass-band. Filtering fabric image with this filter will enhance the normal texture pattern instead of attenuate it. As the half-peak frequency response magnitudes of neighboring filter touch each other in the frequency spectrum, it can be found out that (f_u, f_v) and (-f_u, -f_v) are in the stop-band of all the other Gabor filters.

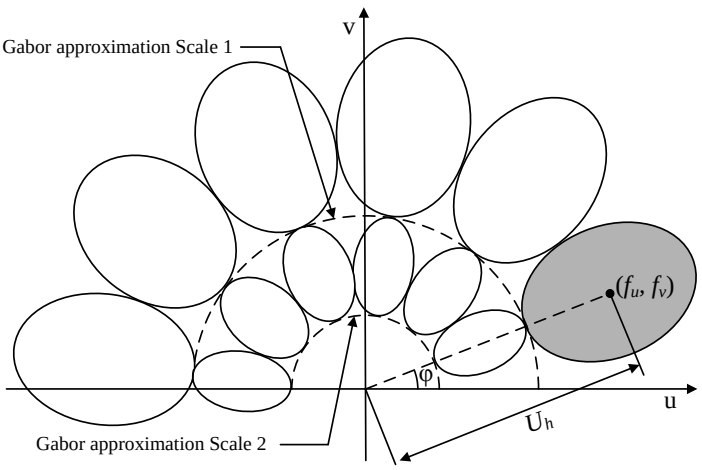

Figure 7. Frequency Response of Modified Gabor Filter Bank

Figure 8, illustrates a sample image with defect *miss-pick* and its filtered image by filter $G_{0,0}$, $G_{1,0}$, $G_{2,0}$. $G_{3,0}$ respectively with (f_u, f_v) = (0.21, 0.07), N = 1, M = 4, $U_h = \sqrt{f_u^2 + f_v^2} = 0.22$. In the image filtered by $G_{0,0}$, the texture pattern is enhanced and the defect is attenuate which is not desirable for defect detection. While in the images filtered by all the other three Gabor filters, the texture backgrounds are effectively attenuated to emphasis the presence of defect, which make it easy to defect. Thus Gabor filter $G_{0,0}$ should not be excluded and all the others in the Gabor filter bank are used for filtering the fabric image.

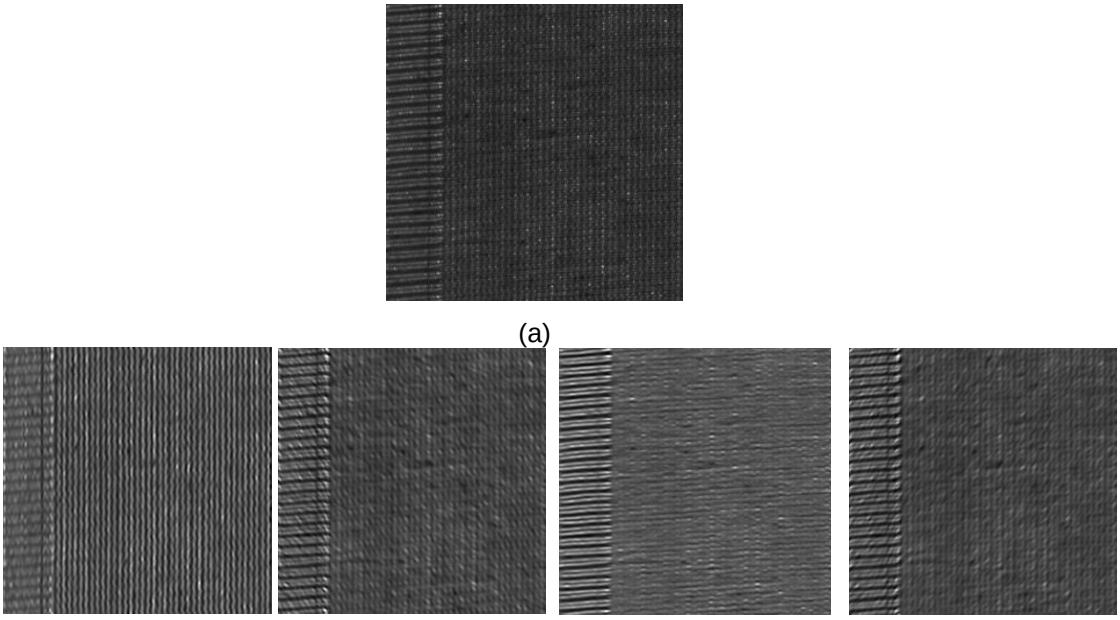

Figure 8. (a) is a Defective Fabric Sample, (b)-(e) are The Filtered Images of (a) Using $G_{0,0}$, $G_{1,0}$, $G_{2,0}$. $G_{3,0}$

4.2. Selection of U_l

As described above, the objective of using Gabor filters is to enhance the energy of defective region and attenuate the energy of normal texture. The attenuation of the normal texture is achieved by analyzing frequency characteristic of non-defective sample fabric image and setting U_h adaptively to the normal texture to make sure that the frequency region corresponding to the normal texture is in the stop-band of all the Gabor filters in the filter bank. Similarly, an intuitive method of selecting U_l is to set it adaptively to make sure that the frequency region corresponding to the defects is in the pass-band of the Gabor filters. However, practically, this is not applicable. Due to the diversity of the fabric defects, the frequency characteristics of defects in a certain fabric are unknown before detection. Different defects may correspond to different frequency regions in frequency domain. Thus the problem of U_l selection is solved in an alternative way.

For standard wavelet transform, the wavelet approximation at scale *i* is further decomposed into wavelet coefficients and wavelet approximation at scale *i+1*. Similarly for Gabor wavelet, its approximation, which can be considered as Gabor approximation , at scale *i* can also be decomposed into Gabor wavelet coefficients and approximation at scale *i+1*. For Gabor approximation at scale i, the Gabor approximation and Gabor wavelet coefficients at scale *i+1* are complimentary to each other (not strictly orthogonally complimentary because of the non-orthogonally of Gabor wavelet). For each scale, the half peak boundary of the Gabor approximation is a circle centered at (0,0) touching the half peak boundary of all the Gabor filters in the same scale as indicated by dash curve in Figure 7. The selection of U_l is determined by examining at which scale of Gabor approximation the normal texture pattern is most effectively attenuated. Figure 9 illustrates a normal fabric texture, and its Gabor approximations from scale 1 to scale 4 with their half peak boundaries set to U_h, $U_h/2$, $U_h/4$ and Uh, $Uh/2$, $Uh/4$ $U_h/8$ respectively. As the scale increases, the texture background in Gabor approximations is increasingly

attenuated. Particularly, the texture pattern in Gabor approximation at scale 3 is almost removed and there is little change between Gabor approximations at scale 3 and scale 4. Because Gabor filters at scale 4 captures the texture information existing in Gabor approximations at scale 3 but not in scale 4 and the texture pattern has already been removed at scale 3, the Gabor filters at scale 4 will not capture any useful texture information. Thus the Gabor filters at scale 4 should not be used and only three scales should be involved for image filtering, that is $U_l = U_h / 4$ in this case.

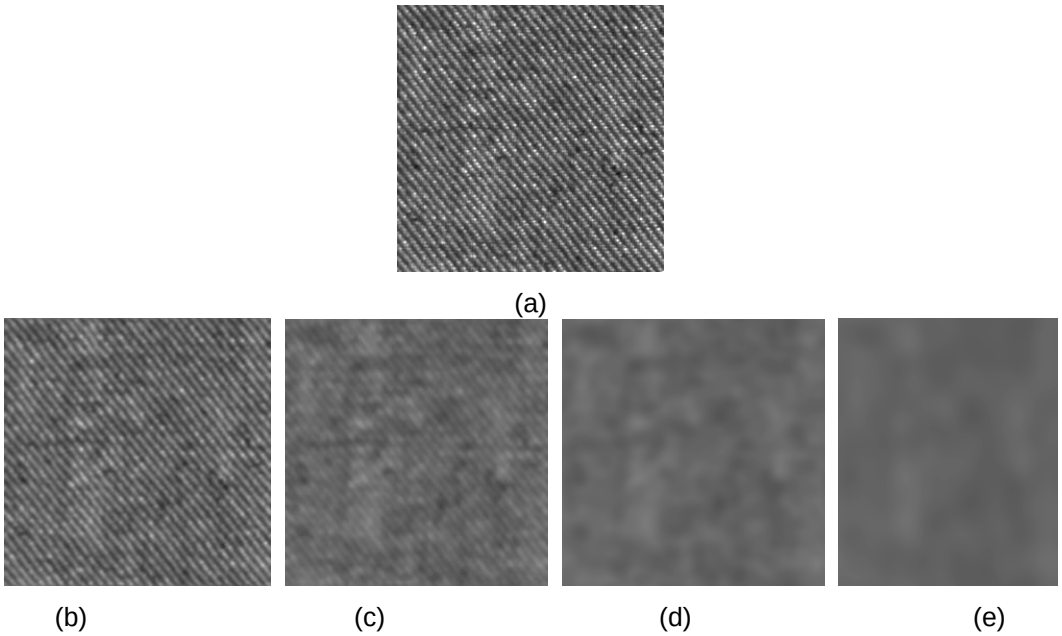

Figure 9. (a) A Normal Fabric Sample, (b)-(e) Gabor Approximations of (a) From Scale 1 to Scale 4

In order to find out the optimal Gabor approximation scale at which the texture is most efficiently attenuated (like scale 3 in Figure 9), a texture feature called gray-level co-occurrence matrix (GLCM) is used to characterize the Gabor approximations at different scales. GLCM estimates image properties related to second-order statistics. A GLCM is a square matrix whose elements correspond to the relative frequency of occurrence of pairs of gray level values of pixels separated by a certain distance in a given direction. The $L \times L$ gray-level co-occurrence matrix Pd for a displacement vector d = (dx, dy) is defined as follows. The entry (i, j) of Pd is the number of occurrences of the pair of gray levels i and j which are a distance d apart. Formally, it is given as

$$P_d(i, j) = \left|\{((x_1, y_1), (x_2, y_2)) : I(x_1, y_1) = i, I(x_2, y_2) = j\}\right| \tag{11}$$

where I denotes an image of size U×V with L gray values, (x_1, y_1), $(x_2, y_2) \in U \times V$, $(x_2, y_2) = (x_1 + dx, y_1 + dy)$ and | . | is the cardinality of a set. Haralick [22] proposed 14 features from GLCM for texture characterization. In this paper, inverse difference moment IDM is used to measure the attenuation degree of the texture background, which is formulated as

$$IDM = \sum_{i=0}^{L-1} \sum_{j=0}^{L-1} \frac{1}{1 + (i - j)^2} p(i, j) \tag{12}$$

IDM can measure the homogeneity of the texture. The more the texture pattern is attenuated, the more homogeneous the texture is, which corresponds to larger value of IDM . Figure 10(a), illustrates the IDM values of Gabor approximation from scale 0 to scale 4 (see Figure 9) with four co-occurrence matrix displacement parameter d = (0,1), (-1,1), (-1,0), (-1,-1), which correspond to 0°, 45°, 90° and 135° respectively. The scale 0 corresponds to the original image in Figure 9(a). Figure 10(b) shows the difference values of IDM from scale 1 to scale 4. It can be seen that the value of IDM increases as the increase of scale, and the optimal scale can be determined by find out at which scale the difference value of IDM reaches its maximum. For four displacement parameters, the $IDMs$ of them all reach their maximum at scale 3. However d = (-1, 1) has the most prominent maximum, because it corresponds to 45°, which is closest to the orientation vertical to the primary orientation of texture pattern, thus it can characterize the texture pattern better than the other three displacement parameters. The primary orientation of the texture pattern can be obtained from the Fourier spectrum of the texture image [9], which can be calculated as 90°-φ.

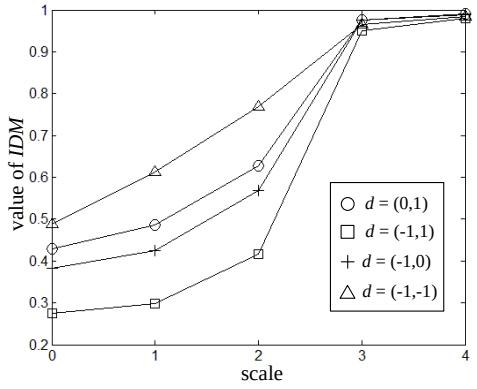

(a)

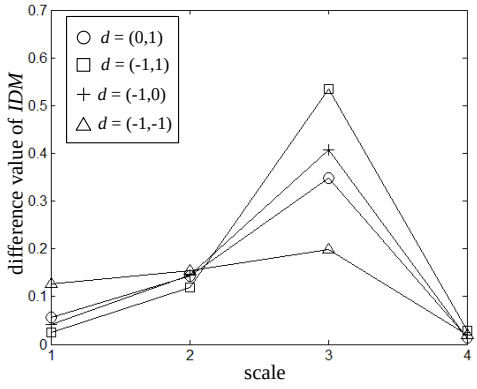

(b)

Figure 10. Value and Difference Value of IDM of Successive Scales in (a),(b) Respectively

Formally, the selection of U_1 can be summarized as following steps. 1) Obtain the Gabor approximation Am (m = 1,2,3,…) with successive scales from a non-defective fabric image sample. The frequency half peak boundaries of each Gabor approximation are set to $U_h / 2m-1,$ where frequency half peak boundaries of the neighboring Gabor approximations are distant by an octave. 2) Calculate the GLCM feature IDM of each Gabor approximation using one of the four displacement

parameters which is closest to the orientation vertical to the primary orientation of texture pattern. 3) Find out the optimal scale p by finding the maximum of difference value of IDM, then $U_l = U_h / 2^{p-1}$.

4.3. Selection of *M* and *N*

Parameter *M* and *N* denote the total number of scales and orientations of the Gabor filter decomposition respectively. *N* is set to 4 empirically, that is four orientations is used for image filtering. *M* is set to $log_2(U_h / U_l) + 1$ to make sure that the center frequency of filters from neighboring scales are placed an octave apart from U_h to U_l.

5. Fabric Defect Detection Algorithm

The flow of the proposed fabric defect detection algorithm is illustrated in Figure 11. Preprocess is used to make the fabric image zero mean to suppress its zero-frequency component in frequency domain. A bank of adaptively tuned Gabor filters (see Section 4) is used to enhance the energy of the defect and attenuate the energy of normal background. As the output the Gabor filter is in complex form containing real and imaginary parts, a non-linear transform $|.|^2$ is used to calculate the energy of pixels in the filtered images.

Different defects correspond to different frequency regions in frequency domain so any Gabor filter in the filter bank can only characterize parts of them. A fusion scheme, as described in [11] is used to fuse the filtered images of all scales and orientations into a single image to emphasize the presence of all kinds of defects. Let $F_{m,n}$ be the image filtered by Gabor filter $G_{m,n}$, then the fused image *S* is calculated by following formulas.

$$R_n(x, y) = \frac{1}{M} \sum_{m=0}^{M-1} F_{m,n}(x, y) \tag{13}$$

$$S(x, y) = \frac{1}{N-1} \sum_{n=0}^{N-2} \left[R_n(x, y) R_{n+1}(x, y) \right]^{1/2} \tag{14}$$

Arithmetic mean is used to fuse the images of all scales in the same orientation and geometric mean is used to fuse the images of different orientations. *M* and *N* denote total scales and orientations respectively. Particularly, $F_{0,0}$ is not involved in the image fusion, because it corresponds to the Gabor filter $G_{0,0}$ which has already been excluded from the filter bank.

The fused image is subjected to thresholding to generate binary images to detect the defective pixels. The threshold value *T* is set to $\mu+\lambda\sigma$, where μ and σ are mean and standard deviation of the fused image of non-defective samples. λ is a parameter compromising between false alarm and miss detection.

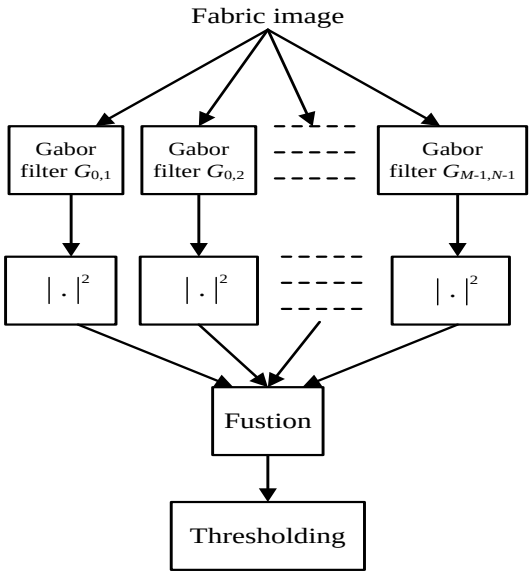

Figure 11. Flow Diagram of Fabric Defect Detection Algorithm

5.1. Results and Discussion

Defects with three categories of texture background containing one plain and two twill fabrics are used to evaluate the performance of the fabric detection algorithm. All the three fabrics and defects on them are produced in factory practice. All of the images are acquired by line scan CCD camera with a spatial resolution of 0.2mm/pixel against a backlighting illumination and digitalized into 256×256 pixels with a gray level of 256. Each of them is considered as one sample for defect detection.

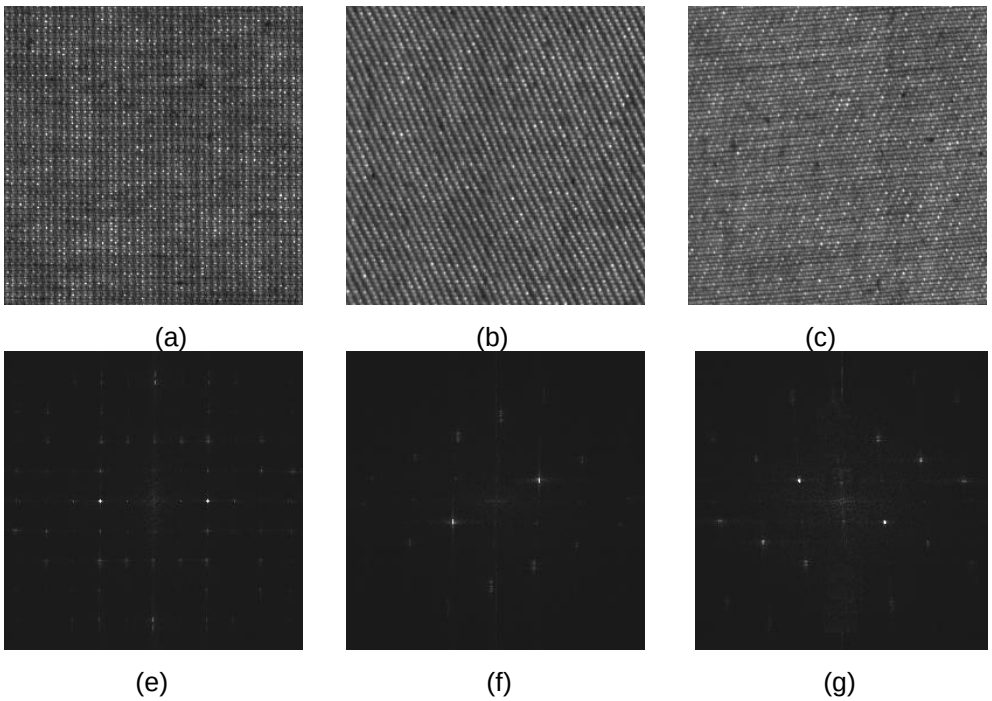

Figure 12. Normal Texture Samples of Three Kinds of Fabrics in (a)-(c) and Their 2-D Fourier Spectrum in (d)-(f)

Figure 12(a)-(c), illustrate the normal texture samples of these three categories of fabrics. It can be seen that there exists two peaks in their 2-D Fourier spectrum in Figure 12(d)-(f), indicating the location of the main energy of the normal texture. The parameters of adaptively tuned Gabor wavelet of three categories of fabric texture are presented in Table 1, where f_u, f_v are normalized frequencies ranging from -0.5 to 0.5. These parameters are obtained from a large non-defective image sample of size 1024×1024 using method described in SEC. The Gabor filtering is implemented by convolution, and the mask size of convolution is set to 7×7.

Table 1. Parameters of Adaptively Tuned Gabor Wavelet of Three Kinds of Fabric Texture

Parameters	Fabric texture Category1	Fabric texture Category2	Fabric texture Category3
Fabric type	plain	twill	twill
Figure NO.	Figure 12(a)	Figure 12(b)	Figure 12(c)
(f_u, f_v)	(0.20, 0.01)	(0.16, 0.13)	(0.15,0.07)
φ	2.9°	39.1°	25.0°
U_h	0.20	0.21	0.17
U_l	0.10	0.11	0.09
M	2	2	2
N	4	4	4

For comparison, two other fabric defect detection algorithms using Gabor filters (described in [10] are also implemented to the experimental fabric image samples. The detection algorithms described in [10] are unsupervised detection methods without using non-defective texture for the adaptive tuning of Gabor filters. They rigidly use the same bank of Gabor filters with fixed parameters to detect fabric defects with all kinds of texture background. In [10], the filter bank consists of 28 Gabor filters containing four orientations 0°, 45°, 90°, 135° and seven scales with (unnormalized) center frequencies $w = \sqrt{2}, 2\sqrt{2}, 4\sqrt{2}, 8\sqrt{2}, 16\sqrt{2}, 32\sqrt{2}, 64\sqrt{2}$ cycles/image-width. While in [11], the filter bank consists of 24 Gabor filters containing 6 orientations 0°, 30°, 60°, 90°, 120°, 150° and four scales with normalized center frequencies W = 1/2, 1/4, 1/8, 1/16. These two algorithms are quite similar with only difference that the center frequencies of Gabor filters in the filter bank are distributed in different locations in frequency domain.

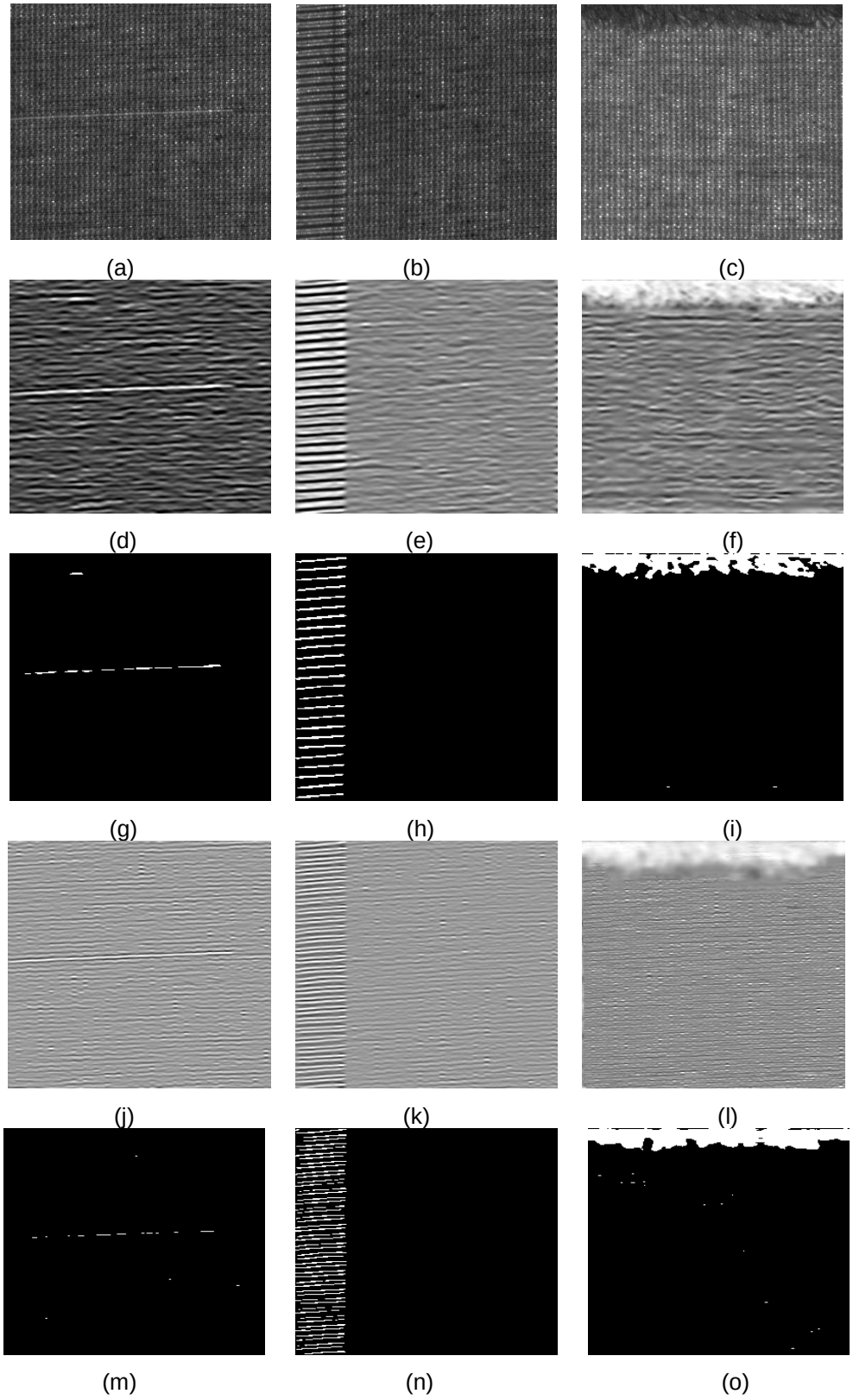

Figure 13. (a)-(c) are Defect Broken Picks, Missing End, Irregular Book in Fabric Texture Category 1; (d)-(f) and (g)-(i) are the Fused Images and Final Detection Results of (a)-(c) Using Proposed Method Respectively; (j)-(l) and (m)-(o) are the Fused Images and Final Detection Results of (a)-(c) Using Method in [10]

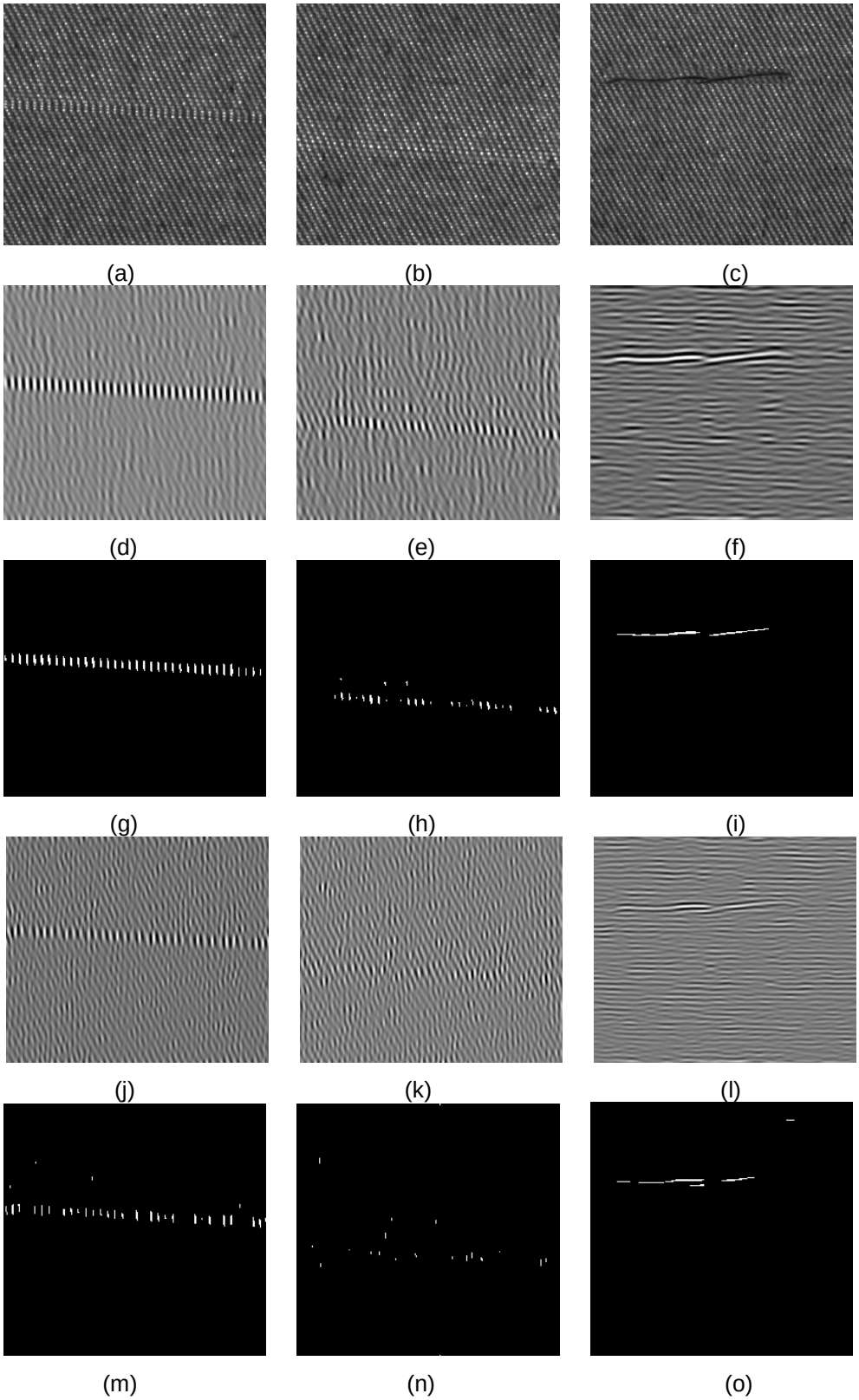

Figure 14. (a)-(c) are Defect Broken Picks, Missing End, Irregular Book in Fabric Texture Category 2; (d)-(f) And (g)-(i) are the Fused Images and Final Detection Results of (a)-(c) Using Proposed Method Respectively; (j)-(l) and (m)-(o) are the Fused Images and Final Detection Results of (a)-(c) Using Method in [11]

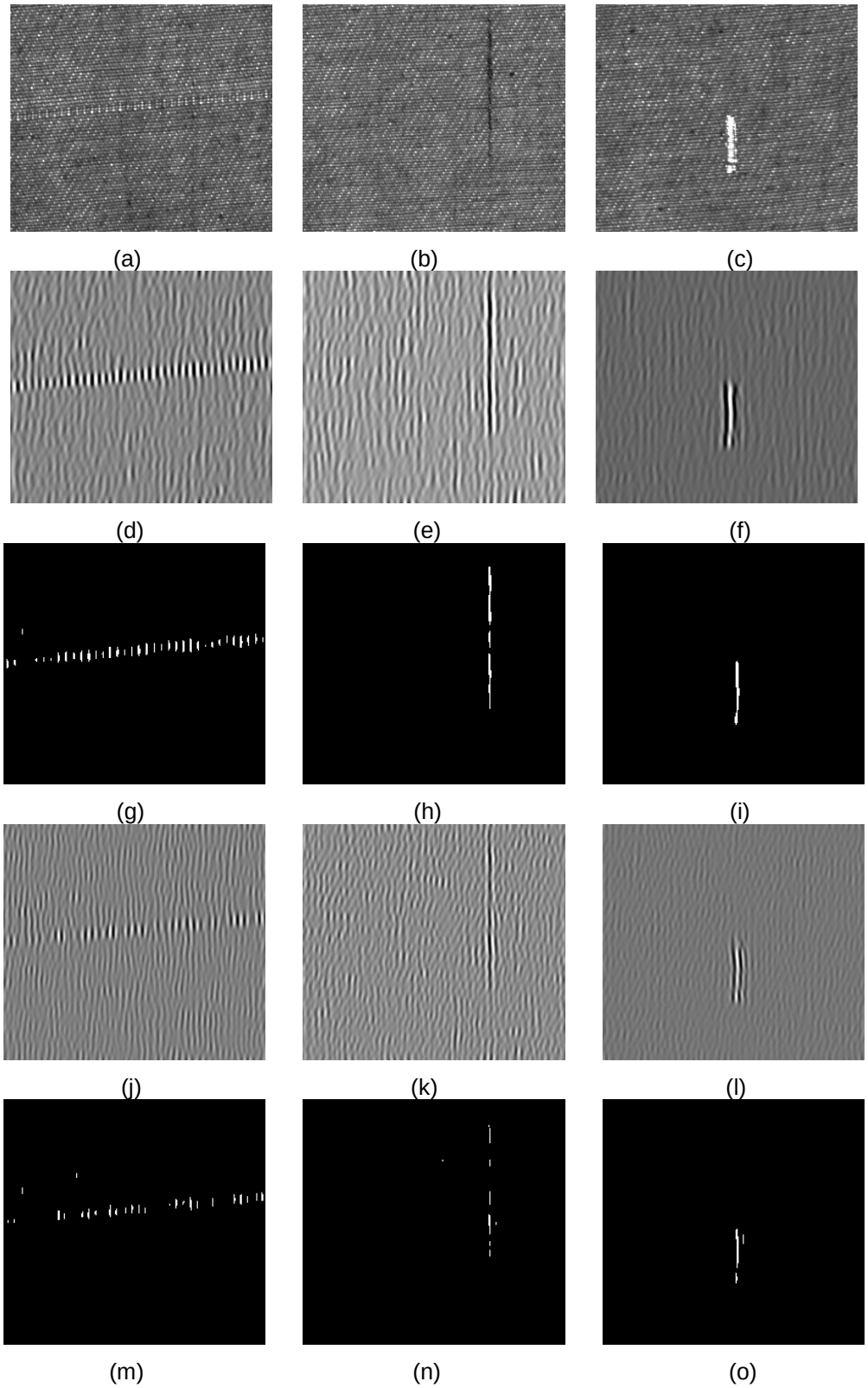

Figure 15. (a)-(c) are Defect Broken Picks, Missing End, Irregular Book in Fabric Texture Category 2; (d)-(f) and (g)-(i) are the Fused Images and Final Detection Results of (a)-(c) Using Proposed Method Respectively; (j)-(l) and (m)-(o) are the Fused Images and Final Detection Results of (a)-(c) Using Method in [11]

Figure 13-15, illustrate several typical defects of three categories of fabric texture and provide a comparison of detection results between three fabric defect detection methods (including our proposed method and methods in [10-11]). It can be seen that in the fused images there are larger distinctions between defective and non-defective texture in our proposed method than the other two methods. Thus our method achieves better detection results. This is because in detection methods in [10] and [11], Gabor filter bank is used rigidly with fixed parameters to detect defects with all kinds of fabric texture rather than tuned adaptively to the fabric texture. Thus some undesirable Gabor filters may be involved in the image filtering which may lead to the enhancement of normal texture and attenuation of defective regions (as illustrated in Figure 8(b)). And this will bring negative effects to the final detection results, particularly in Figure 13(m), and Figure 14(n), which indicate the failure of .detection using methods in [10-11].

Table 2, presents the detection accuracy of thee detection methods. It can be seen that our method achieves better detection accuracy than the other two methods. Besides, the Gabor filter bank in [10-11] is used to cover the whole frequency domain, so multiply Gabor filters (28 and 24 respectively) are involved in image filtering which leads to large computational load. However, in our proposed the Gabor filter bank only covers only parts of the frequency regions in frequency domain (from U_l to U_h). As indicated in Table 1, only 8 Gabor filters (2 scales and 4 orientations) are used for all three categories of fabric texture. Thus our proposed method has less computational complexity and has better real-time performance.

Table 2. Detection Results of Three Detection Methods

Fabric category	defective samples	detection accuracy		
		proposed method	method in [10]	method in [11]
1	33	93.9%	90.9%	87.9%
2	41	92.7%	85.3%	87.8%
3	37	97.3%	86.5%	89.2%
total	111	94.6%	87.4%	88.3%

Compared to the detection method in [10] the proposed method uses an extra non-defective image sample for prior learning to obtain the frequency characteristics of the fabric texture and adaptive tuning of Gabor filters. However, because the non-defective samples of the fabric image are usually readily to get (even in practical factory occasions), thus our method will not bring any actual inconvenience in detection progress but gets better detection accuracy and real-time performance.

6. Conclusions

A new method of fabric defect detection using Gabor filters been demonstrated. In order to emphasize the presence of defects, a new Gabor wavelet tuning method is used to enhance the energy of defective region and attenuate the energy of normal texture. As a major contribution of this work, the parameters of Gabor wavelet are tuned adaptively to the spectral characteristics of normal texture which is obtained from non-defective fabric samples. The performances of the proposed method and two other Gabor filter based detection methods without adaptive tuning have been evaluated by defect samples with different texture backgrounds. The results indicate

that the proposed method has better detection accuracy and real-time performance, thus is more suitable for the implementation of industrial inspection.

Acknowledgments

This project supported by Nature Science Foundation of Hubei Province (2014CFB485) and the Fundamental Research Funds for the Central Universities (WUT: 2014-IV-076)

References

[1] K. Srinivasan, P. H. Dastor, P. Radhakrishnaihan and S. Jayaraman, "FDAS: A knowledge-based frame detection work for analysis of defects in woven textile structures", Text. Inst., vol. 83, no. 3, **(1992)**, pp. 431-447.
[2] H. S. Sarraf and J. S. Goddard, "Vision systems for on-loom fabric inspection", IEEE Trans. Ind. Appl., vol. 35, no. 6, **(1999)**, pp. 1252-1259.
[3] A. Conci and C. B. Proenca, "A fractal image analysis system for fabric inspection based on a box-counting method", Computer Networks & ISDN Systems, vol. 30, no. 98, **(1998)**, pp. 1887-1895.
[4] H. G. Bu, J. Wang and X. B. Huang, "Fabric defect detection based on multiple fractal features and support vector data description", Engineering Applications of Artificial Intelligence, vol. 22, no. 2, **(2009)**, pp. 224-235.
[5] B. M. Goswami, and A. K. Datta, "Detecting defects in fabric with laser-based morphological image processing", Text. Res., vol. 70, no. 9, **(2000)**, pp. 758-762.
[6] J. K. Chandra, P. K. Banerjee and A. K. Dattab, "Neural network trained morphological processing for the detection of defects in woven fabric", Text. Inst., vol. 1, no. 101, **(2010)**, pp. 699-706.
[7] A. L. Amet, A. Ertuzun and A. Ercil, "An efficient method for texture defect detection: sub-band domain co-occurrence matrices", Image and Vision Computing, vol. 18, no. 6-7, **(2000)**, pp. 543-553.
[8] F. S. Cohen, Z. Fan and S. Attali, "Automated inspection of textile fabrics using textural models", IEEE Trans. Pattern Anal. Mach. Intell., vol. 8, no. 13, **(1991)**, pp. 803-808.
[9] C. H. Chan and G. K. H. Pang, "Fabric defect detection by Fourier analysis", IEEE Trans. Industry Applications, vol. 36, no. 5, **(2000)**, pp. 1267-1276.
[10] A. K. Jain and F. Farrokhnia, "Unsupervised Texture Segmentation Using Gabor Filters", Pattern Recognition, vol. 24, no. 2, **(1991)**, pp. 1167-1186.
[11] A. Kumar and G. Pang, "Defect detection in textured materials using optimized Gabor filters", IEEE Trans. Syst., Man, Cybern. B, Cybern., vol. 32, no. 5, **(2002)**, pp. 553-570.
[12] K. L. Mak and P. Peng, "Detecting defects in textile fabrics with optimal Gabor filters", Int. J. Comput. Sci. 1, vol. 1, no. 1, **(2006)**, pp. 1306–4428.
[13] A. Bodnarova, M. Bennamoun and S. J. Latham, "Optimal Gabor filters for textile flaw detection", Pattern Recognit., vol. 35, no. 12, **(2002)**, pp. 2973-2991.
[14] K. L. Mak and P. Peng, "An automated inspection system for textile fabrics based on Gabor filters", Robot Comput. Integr. Manuf., vol. 24, no. 3, **(2008)**, pp. 359-369.
[15] W. J. Jasper, S. J. Garnier and H. Potapalli, "Texture characterization and defect detection using adaptive wavelets", Opt. Eng., vol. 35, no. 11, **(1996)**, pp. 3140-3149.
[16] X. Z. Yang, G. Pang and N. Yung.. "Fabric defect detection using adaptive wavelet", ICASSP IEEE Int Conf Acoust Speech Signal Process Proc in Proc. Salt Lake, vol. 6, no. 12, **(2001)**, pp. 3697-3700.
[17] X. Yang, G. Pang and N. Yung, "Discriminative fabric defect detection using adaptive wavelets", Optical Engineering, vol. 41, no. 12, **(2002)**, pp. 3116-3126.
[18] R. De Valois, D. Albrecht and L. Thorell, "Spatial-frequency selectivity of cells in acaque visual cortex", Vision Research, vol. 1, no. 22 , **(1982)**, pp. 545–559.
[19] M. Unser, "Texture classification and segmentation using wavelet frames", IEEE Trans. Image Processing, vol. 4, no. 11, **(1995)**, pp. 1549–1560.
[20] T. S. Lee, "Image representation using 2D Gabor wavelets", IEEE Trans. Pattern Analysis and Machine Intelligence, vol. 18, no. 10, **(1996)**, pp. 959–971.
[21] B. S. Manjunath and W. Y. Ma, "Texture features for browsing and retrieval of image data", IEEE Trans. Pattern Anal. Machine Intell., vol. 18, no. 8, **(1996)**, pp. 837–842.
[22] R. M. Haralick, "Statistical and structural approaches to texture", Proceedings of the IEEE, vol. 67, no. 5, **(1979)**, pp. 786-804.

Author

LuoJie (1983) is a lecturer in Wuhan University of Technology, China. He received his Ph.D. degree in Communication and Information Engineering at the Wuhan University of Technology, China, in 2013. His research interests are Imagine Processing and Communication System of Vehicle.